Available online at www.sciencedirect.com
SCIENCE DIRECT®
Journal of Power Sources 140 (2005) 72–80
JOURNAL OF POWER SOURCES
www.elsevier.com/locate/jpowsour

Valveless piezoelectric micropump for fuel delivery in direct methanol fuel cell (DMFC) devices

Tao Zhang, Qing-Ming Wang*

Department of Mechanical Engineering, University of Pittsburgh, Pittsburgh, Pennsylvania, PA 15261, USA

Received 22 June 2004; accepted 18 July 2004
Available online 30 November 2004

Abstract

Fuel cells are being considered as an important technology that can be used for various power applications. For portable electronic devices such as laptops, digital cameras, cell phone, etc., the direct methanol fuel cell (DMFC) is a very promising candidate as a power source. Compared with conventional batteries, DMFC can provide a higher power density with a long-lasting life and recharging which is almost instant. However, many issues related to the design, fabrication and operation of miniaturized DMFC power systems still remain unsolved. Fuel delivery is one of the key issues that will determine the performance of the DMFC. To maintain a desired performance, an efficient fuel delivery system is required to provide an adequate amount of fuel for consumption and remove carbon dioxide generated from fuel cell devices at the same time. In this paper, a novel fuel delivery system combined with a miniaturized DMFC is presented. The core component of this system is a piezoelectric valveless micropump that can convert the reciprocating movement of a diaphragm activated by a piezoelectric actuator into a pumping effect. Nozzle/diffuser elements are used to direct the flow from inlet to outlet. As for DMFC devices, the micropump system needs to meet some specific requirements: low energy consumption but a sufficient fuel flow rate. Based on theoretical analysis, the effect of piezoelectric materials properties, driving voltage, driving frequency, nozzle/diffuser dimension, and other factors on the performance of the whole fuel cell system will be discussed. As a result, a viable design of a micropump system for fuel delivery can be achieved and some simulation results will be presented as well.

Keywords: Piezoelectric valveless micropump; Direct methanol fuel cell; Fuel delivery

1. Introduction

Many portable electronic devices available to consumers nowadays are combining more and more functionalities together. Consequently, the power consumption of these devices is consistently increasing. Although a great amount of effort has already been put into the research on the improvements of conventional rechargeable batteries, the performance of these power devices is still unsatisfactory. On the other hand, as reported by Hebling et al. [1], portable and miniaturized fuel cells have shown many advantages over the batteries, such as higher power density, instant recharging, low environmental impacts etc. So, it becomes very possible to use fuel cell as a portable power source instead of batteries in the near future.

Among various types of fuel cells, the proton exchange membrane fuel cell (PEMFC) and DMFC are applicable for the portable electronics due to their low operation temperature. In comparison with DMFC, the PEMFC device that uses hydrogen directly as fuel has a better performance, but suffers from the storage problem of hydrogen. So far the storage and transportation of hydrogen are still not cost-effective for commercial applications. And the fuel cell with a reformer to convert the liquid fuel to hydrogen gas is also less favorable because it increases the complexity of the system integration and generates undesired byproduct (carbon monoxide, CO) during the reforming process. Therefore, a DMFC using a liq-

* Corresponding author. Tel.: +1 412 624 4885; fax: +1 412 624 4846.
E-mail address: qmwang@engr.pitt.edu (Q.-M. Wang).

0378-7753/$ – see front matter © 2004 Elsevier B.V. All rights reserved.
doi:10.1016/j.jpowsour.2004.07.026

uid methanol solution as fuel directly is much more straightforward and attractive. Many researchers including Waidhas et al. [2] and Scott et al. [3] have discussed the benefits and challenges, utilizing such a direct-fuelled system.

To optimize a miniaturized DMFC power system, many engineering issues need to be considered which include thermal management, methanol crossover, fuel delivery, oxidant supply and power conditioning. This paper mainly focuses on the fuel delivery. For medium- and large-size DMFC, conventional pumps can be used to drive the fuel flowing through the fuel cell. For miniaturized DMFC, the flow rate of fuel is very small and there are several options for fuel delivery. Mench et al. [4] presented a pump-less and self-activated design for a DMFC stack, in which gravitational and capillary forces were used to feed the liquid methanol solution. By their calculation, the fuel supply rate was adequate for acceptable performance. This design was quite interesting and simple but no experimental results were reported. In addition, the fabrication of the DMFC stack seems to be very complicated. The more general way is to choose a micropump. Both Shukla et al. [5] and Scott et al. [6] used a peristaltic pump in their experimental study. The flow rate of fuel varied from less than 1 to 5 ml min^{-1} and the active cell area ranged from 9 to 25 cm^2. The operation performance of their fuel cell systems was in the acceptable range. Therefore, it seems to be more practical and easier to employ a micropump for fuel delivery.

The research on micropumps started from 1980s and various designs have been presented since then. Olsson [7] summarized the performance of several typical micropumps. Among them the reciprocating diaphragm pumps show a broad range of pumping flow rate and can be easily fabricated using a MEMS technique. To eliminate the wearing and fatigue of valves and reduce clogging, a valveless design is preferred. Stemme E. and Stemme G. [8] introduced the first piezoelectric valveless micropump. Gerlach et al. [9] presented a similar type of micropump using different flow directing elements. Forster et al. [10] compared the performance between the micropump with diffuser and the micropump with valvular conduit. It was found that the valvular conduit design had a higher volumetric efficiency. Olsson [7] and Ullmann [11] also conducted fairly extensive modeling and experimental research on this valveless micropump. Based on these previous studies, a new fuel delivery system for miniaturized DMFC using a piezoelectric valveless micropump is presented in this paper. The performance of this system is analyzed theoretically.

2. System design

The cross-section of the DMFC power system with piezoelectric micropump is shown schematically in Fig. 1. Note that the figure is not drawn in the actual scale. This system mainly consists of the following parts: fuel cell membrane electrode assembly (MEA), fuel chamber, nozzle/diffuser, micropump and pump chamber, and fuel supply manifold. All these parts are fabricated in a multilayer structure to obtain a compact fuel cell system. The fuel cell MEA is made of a Nafion® 117 membrane layer sandwiched by two electrode layers with catalysts deposited on them. And the micropump is fabricated by adhering a thin piezoelectric disk on to a metal diaphragm. When applying an alternating voltage to the piezoelectric disk, the diaphragm is actuated to produce bending deformation that causes volume change in pump chamber. By selecting an appropriate shape and dimension of the nozzle/diffuser between the pump chamber and the fuel chamber, the fuel can circulate in the desired direction. And the fuel supply from the right chamber can compensate for the fuel consumption.

3. Model of micropump

As shown in Fig. 2, the vibrating diaphragm on top of the pump chamber is actually a piezoelectric bending mode actuator with fixed edges. Both applied voltage across the PZT disk, U, and pressure difference exerted on the whole diaphragm, p, can cause the deflection in vertical direction. Specifically p is the difference between the pressure above the pump diaphragm (usually the atmospheric pressure) and the pressure below the pump diaphragm (the pressure of the pump chamber).

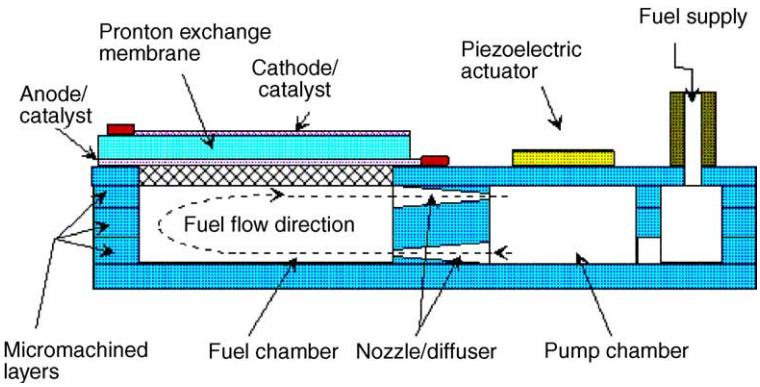

Fig. 1. Schematic of the miniaturized DMFC system driven by piezoelectric valveless micropump.

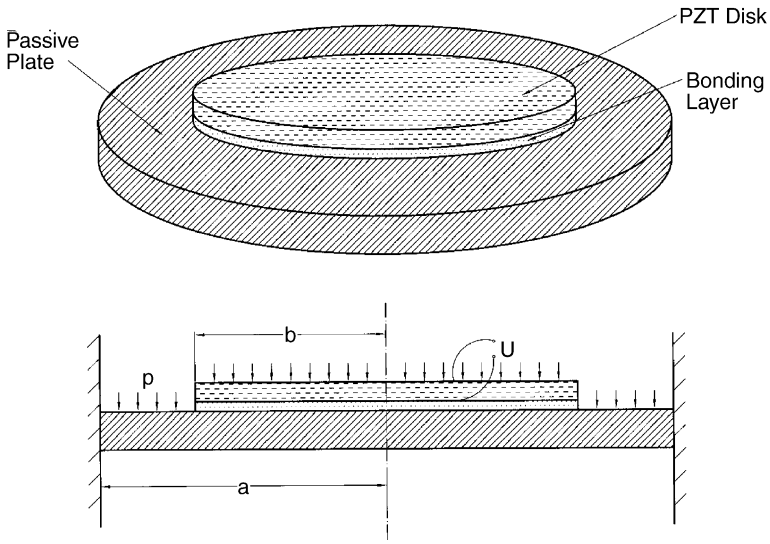

Fig. 2. Schematic of the piezoelectric micropump actuator.

A theoretical model developed by Li and Chen [12] is adopted to estimate the deflection induced by the applied voltage. According to their study, this analytical solution is able to predict reasonable deflections for the passive plates of various Young's modulus from 30 to 600 GPa. The passive plate used in this design is well within this range. To simplify the modeling process, the piezoelectric pump actuator is divided into two parts: one is the three-layer structure including the PZT disk, the bonding layer and the passive metal plate; the other is the rest part of the passive plate.

From Li and Chen [12], the deflections of the three-layer structure and the rest part of the passive plate can be calculated separately. For the rest part of the passive plate, its deflection W_1 is obtained using the equations given by Timoshenko et al. [13]

$$W_1(r) = \frac{M_{11}b^2}{2D_{\mathrm{p}}[(1-\gamma_{\mathrm{p}})a^2+(1+\gamma_{\mathrm{p}})b^2]} \times \left(-r^2+2a^2\log\frac{r}{a}+a^2\right) \quad (1)$$

For the three-layer structure, its deflection W_2 also follows Timoshenko et al. [13]

$$W_2(r) = \frac{M_{11}b^2}{2D_{\mathrm{p}}[(1-\gamma_{\mathrm{p}})a^2+(1+\gamma_{\mathrm{p}})b^2]} \times \left(-b^2+2a^2\log\frac{b}{a}+a^2\right)+\frac{M_1}{2D_{\mathrm{c}}(1+\gamma_{\mathrm{c}})}(b^2-r^2) \quad (2)$$

Here, a and b represent the radius of the passive plate and the PZT disk respectively. D_{p} and γ_{p} are the flexural modulus and Poisson's ratio of the passive plate. D_{c} and γ_{c} are the flexural modulus and Poisson's ratio of the three-layer structure. M_1 and M_{11} are intermediate bending moments.

The bending moment M_1, as derived by Li and Chen [12], is

$$M_1 = \frac{\eta U d_{31}(2h'+2h_{\mathrm{b}}+h_{\mathrm{pzt}})(h'^3+h^3)}{2[h^3+(1-\alpha)h'^3+(\alpha-\beta)(h'+h_{\mathrm{b}})^3 +\beta(h'+h_{\mathrm{b}}+h_{\mathrm{pzt}})^3]} \quad (3)$$

Here, U is the static voltage applied on the PZT disk, d_{31} is the piezoelectric charge coefficient, and h is the location of the neural surface of the three-layer structure. The equations for other variables are:

$$h' = h_{\mathrm{p}}-h, \quad \alpha = \frac{1-\gamma_{\mathrm{p}}^2}{1-\gamma_{\mathrm{b}}^2}\frac{E_{\mathrm{b}}}{E_{\mathrm{p}}},$$

$$\beta = \frac{1-\gamma_{\mathrm{p}}^2}{1-\gamma_{\mathrm{pzt}}^2}\frac{E_{\mathrm{pzt}}}{E_{\mathrm{p}}}, \quad \eta = \frac{E_{\mathrm{pzt}}}{1-\gamma_{\mathrm{pzt}}^2}$$

where E_{p}, E_{b}, and E_{pzt} represent the Young's modulus of the passive plate, the bonding layer and the PZT disk, respectively. γ_{p}, γ_{b}, and γ_{pzt} represent the Poisson's ratio of the passive plate, the bonding layer and the PZT disk, respectively. h_{p}, h_{b}, and h_{pzt} represent the thickness of the passive plate, the bonding layer and the PZT disk, respectively.

Based on the work done by Dobrucki et al. [14], the location of the neutral surface of the three-layer structure, h, can be calculated by

$$h = \frac{1}{2}\frac{E_{\mathrm{p}}h_{\mathrm{p}}^2/(1-\gamma_{\mathrm{p}}^2)+E_{\mathrm{b}}[(h_{\mathrm{p}}+h_{\mathrm{b}})^2-h_{\mathrm{p}}^2]/(1-\gamma_{\mathrm{b}}^2) +E_{\mathrm{pzt}}[(h_{\mathrm{p}}+h_{\mathrm{b}}+h_{\mathrm{pzt}})^2-(h_{\mathrm{p}}+h_{\mathrm{b}})^2]/(1-\gamma_{\mathrm{pzt}}^2)}{E_{\mathrm{p}}h_{\mathrm{p}}/(1-\gamma_{\mathrm{p}}^2)+E_{\mathrm{b}}h_{\mathrm{b}}/(1-\gamma_{\mathrm{b}}^2)+E_{\mathrm{pzt}}h_{\mathrm{pzt}}/(1-\gamma_{\mathrm{pzt}}^2)} \quad (4)$$

By observing Eqs. (1) and (2), it can be found that the continuity of deflection at $r = b$ is already satisfied. So, the continuity condition of the slope of the deflection at $r = b$ has to be used to determine unknown moment M_{11}.

To satisfy the continuity condition,

$$\left.\frac{dW_1(r)}{dr}\right|_{r=b} = \left.\frac{dW_2(r)}{dr}\right|_{r=b} \quad (5)$$

Substituting Eqs. (1) and (2) into Eq. (5), the moment M_{11} is found to be

$$M_{11} = -\frac{M_1 D_p[(1-\gamma_p)a^2 + (1-\gamma_p)b^2]}{D_c(1+\gamma_c)(a^2-b^2)} \quad (6)$$

Substituting Eq. (6) back into Eqs. (1) and (2), the whole deflection can be rewritten as

$$W_1(r) = \frac{M_1 b^2(r^2 - 2a^2\log r/a - a^2)}{2D_c(1+\gamma_c)(a^2-b^2)}, \quad (b \le r \le a) \quad (7)$$

$$W_2(r) = \frac{M_1[(a^2-b^2)(b^2-r^2) + b^2(b^2 - 2a^2\log b/a - a^2)]}{2D_c(1+\gamma_c)(a^2-b^2)}, \quad (0 \le r \le b) \quad (8)$$

The deflection caused by pressure difference can be evaluated using the similar method. Under constant pressure difference p, the deflection of the rest part of the passive plate is

$$W_3(r) = \frac{p}{64D_p}(a^2-r^2)^2 + \frac{(M_{21}-M_2)b^2(r^2 - 2a^2\log r/a - a^2)}{2D_p[(1-\gamma_p)a^2 + (1+\gamma_p)b^2]} \quad (9)$$

The deflection of the three-layer structure is

$$W_4(r) = \frac{p}{64D_p}(a^2-b^2)^2 + \frac{(M_{21}-M_2)b^2(b^2 - 2a^2\log b/a - a^2)}{2D_p[(1-\gamma_p)a^2 + (1+\gamma_p)b^2]} + \frac{p(b^2-r^2)}{64D_p}\left(\frac{5+\gamma_c}{1+\gamma_c}b^2 - r^2\right) + \frac{M_2}{2D_c(1+\gamma_c)}(b^2-r^2) \quad (10)$$

Here, M_2 and M_{21} are also two intermediate bending moments, of which

$$M_{21} = \frac{p}{16}[(1+\gamma_p)a^2 - (3+\gamma_p)b^2] \quad (11)$$

Similar to the case of the deflection due to piezoelectric effect, the continuity of deflection at $r = b$ is already satisfied in Eqs. (9) and (10). And the continuity condition of the slope of the deflection at $r = b$ can be used to determine the other moment M_2.

The volume change of the pump chamber induced by the deflection of the pump diaphragm can be calculated using

$$\Delta V = 2\pi \int_0^R W(r) r\, dr \quad (12)$$

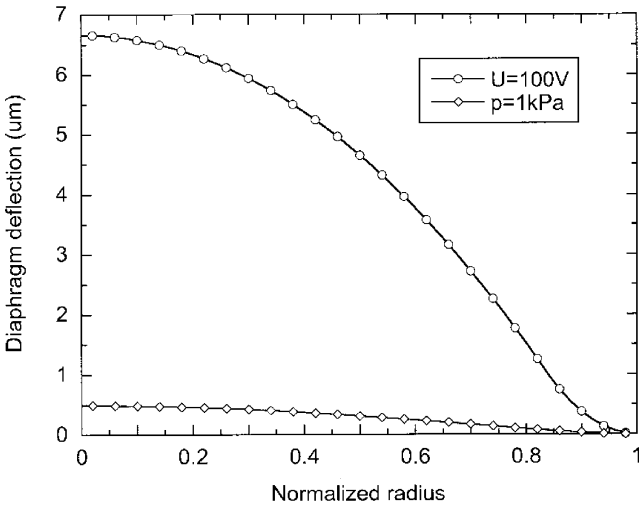

Fig. 3. Comparison of the diaphragm deflections under 100 V and 1 kPa.

The total deflection of the pump diaphragm is the superposition of the deflection introduced by applied voltage and the deflection caused by pressure difference. In actual pump applications, the applied voltage can be easily controlled while the pressure of the pump chamber is coupled with the deflection of the pump diaphragm and flow resistance. Numerical iteration methods can be used to determine the deflection of the pump diaphragm precisely.

For this design, several kPa of pressure difference between the fuel chamber and the pump chamber should be enough to drive the fuel circulating between them. If the pressure of the fuel chamber is kept at the atmospheric pressure, the pressure difference between the pump chamber and the atmospheric pressure is also in the range of several kPa. Using Eqs. (7)–(10), the deflection under 100 V of applied voltage and the deflection under 1 kPa of pressure difference are calculated separately and the results are shown in Fig. 3. The dimensions and material properties of the pump actuator listed in Table 1 are used for calculation. In comparison with the deflection induced by applied voltage, the deflection caused by pressure difference is small and the resultant volume change is smaller. Therefore, the effect of the pressure difference on the volume change is neglected to obtain an analytical solution.

Table 1
Dimensions and material properties of the piezoelectric micropump actuator

	Piezoelectric disk (PZT-5H)	Bonding layer (conductive epoxy)	Passive plate (steel)
Diameter (mm)	20	20	24
Thickness (mm)	0.2	0.02	0.25
Young's modulus (Pa)	6.2×10^{10}	5.17×10^{9}	1.95×10^{11}
Poisson's ratio	0.31	0.3	0.3
d_{31} ($m\,V^{-1}$)	-3.2×10^{-10}		
ε_{33}^{T} ($F\,m^{-1}$)	2.856×10^{-8}		

Due to this simplification, the total deflection of the pump diaphragm can be expressed as

$$W(r) = \begin{cases} W_2(r), & 0 \le r < b; \\ W_1(r), & b \le r \le a; \end{cases} \quad \text{and} \quad R = a. \tag{13}$$

Substituting Eq. (13) into Eq. (12), the volume change of the pump chamber is obtained

$$\Delta V = \frac{\pi}{2}\left[k_A b^4 + 2k_B b^2 + k_C\left(a^4 - b^4 + 4a^2b^2\log\frac{b}{a}\right)\right] \tag{14}$$

Here,

$$k_A = \frac{M_1}{2D_c(1+\gamma_c)}, \quad k_B = \frac{M_1 b^2(b^2 - 2a^2\log b/a - a^2)}{2D_c(1+\gamma_c)(a^2-b^2)},$$

$$k_C = \frac{M_1 b^2}{2D_c(1+\gamma_c)(a^2-b^2)}$$

It is obvious that these coefficients k_A, k_B, k_C, are proportional to M_1. On the other hand, M_1 is proportional to the applied voltage U. Therefore, the volume change ΔV is ultimately proportional to the applied voltage U, which can be written as

$$\Delta V = k_{\text{eff}} U \tag{15}$$

The proportional coefficient is given by

$$k_{\text{eff}} = \frac{\pi}{2} k_U\left[k'_A b^4 + 2k'_B b^2 + k'_C\left(a^4 - b^4 + 4a^2b^2\log\frac{b}{a}\right)\right] \tag{16}$$

Here,

$$k'_A = \frac{1}{2D_c(1+\gamma_c)}, \quad k'_B = \frac{b^2(b^2 - 2a^2\log b/a - a^2)}{2D_c(1+\gamma_c)(a^2-b^2)},$$

$$k'_C = \frac{b^2}{2D_c(1+\gamma_c)(a^2-b^2)},$$

$$k_U = \frac{\eta d_{31}(2h' + 2h_b + h_{pzt})(h'^3 + h^3)}{2[h^3 + (1-\alpha)h'^3 + (\alpha-\beta)(h'+h_b)^3 + \beta(h'+h_b+h_{pzt})^3]}$$

If an alternating sinusoidal voltage is applied to the piezoelectric disk and the actuation frequency is far lower than the resonance frequency of the pump, U can be substituted by $U_m \sin(\omega t)$. U_m is the amplitude of the sinusoidal voltage applied on the piezoelectric plate and ω is the angular frequency.

To estimate the net flow rate of the pump, the modeling of the nozzle/diffuser is also necessary. As mentioned before, these nozzle/diffuser elements can directly flow from inlet to outlet. They are geometrically designed to have a lower pressure loss in one direction than in the opposite direction for the same flow velocity. The characteristic of nozzle/diffuser element can be described as follows,

$$\Delta p = \tfrac{1}{2}\rho v^2 \xi \tag{17}$$

Here, Δp is the pressure loss through the nozzle/diffuser element, ρ is the density of the fluid, v is the velocity of the fluid, and ξ is the pressure loss coefficient. And it can also be expressed in the form of flow rate Q,

$$Q = C\sqrt{\Delta p} \tag{18}$$

Here, C is called conductivity coefficient. Two different flow directions correspond to two different C values. One is higher than the other. The conductivity coefficient in positive direction is represented by C_H and the conductivity coefficient in negative direction is represented by C_L. Accordingly, there are also two different ξ values: the pressure loss coefficient in positive direction is represented by ξ_{positive} and the conductivity coefficient in negative direction is represented by ξ_{negative}.

As mentioned before, it is assumed that the effect of the pressure difference on the volume change is negligible, and thus only the volume change induced by applied voltage is considered. Also assume that there is no pressure variance throughout each chamber so that the pressures of the pump chamber and the fuel chamber can be represented as p_p and p_f, respectively. Given these assumptions, the equations derived by Ullmann [15] can be used to obtain the analytical solutions for the fuel flow rate and the pressure of the pump chamber. The pressure of the fuel chamber is set to be the atmospheric pressure.

(1) Pump mode: $p_p > p_f$

$$Q_1 = \frac{C_L}{C_H + C_L} k_{\text{eff}} U_m \omega \cos(\omega t) \tag{19}$$

$$Q_2 = \frac{C_H}{C_H + C_L} k_{\text{eff}} U_m \omega \cos(\omega t) \tag{20}$$

$$p_p = p_f + \left[\frac{k_{\text{eff}} U_m \omega \cos(\omega t)}{C_H + C_L}\right]^2 \tag{21}$$

(2) Supply mode: $p_p < p_f$

$$Q_1 = -\frac{C_H}{C_H + C_L} k_{\text{eff}} U_m \omega \cos(\omega t) \tag{22}$$

$$Q_2 = -\frac{C_L}{C_H + C_L} k_{\text{eff}} U_m \omega \cos(\omega t) \tag{23}$$

$$p_p = p_f - \left[\frac{k_{\text{eff}} U_m \omega \cos(\omega t)}{C_H + C_L}\right]^2 \tag{24}$$

The average net flow rate is given by

$$\bar{Q} = \frac{k_{\text{eff}} U_m \omega}{\pi} \frac{C_H - C_L}{C_H + C_L} = \frac{k_{\text{eff}} U_m \omega}{\pi} \frac{\eta^{1/2} - 1}{\eta^{1/2} + 1} \tag{25}$$

Here, $\eta = \xi_{\text{negative}}/\xi_{\text{positive}} = (C_H/C_L)^2$

Since the electrical power used to drive the micropump comes from the fuel cell itself, it is necessary to estimate how much energy the micropump needs to consume. Electrically the bending piezoelectric actuator behaves like a planar capacitor. The electric capacitance under the given mechanical boundary condition is very complicated. In a similar case, the capacitance of a circular PZT actuator with clamped edges has given by Kim et al. [16]

$$C = \frac{\varepsilon_{33}^{\mathrm{T}}\pi b^2}{h_{\mathrm{pzt}}} \times \left\{1-\frac{2}{1-\nu}\left[1-\frac{3(s_{11}^{\mathrm{E}})^2 s_{\mathrm{p}} h_{\mathrm{p}}^2 h_{\mathrm{pzt}}(h_{\mathrm{pzt}}+h_{\mathrm{p}})^2}{S_h B_{31}}\right] K_{31}^2\right\} \quad (26)$$

Here, $\varepsilon_{33}^{\mathrm{T}}$ is the permittivity of the PZT disk. s_{11}^{E} is the elastic compliance of the PZT disk at constant electric field and s_{p} is the elastic compliance of the passive layer. K_{31} is the electromechanical coupling coefficient of the PZT disk. v is the Poisson's ratio. Kim et al. [16] assume that the Poisson's ratio of the PZT disk is the same as that of the passive plate and the effect of the bonding layer on the capacitance is neglected. The equations for the other two parameters are:

$$S_{\mathrm{h}} = h_{\mathrm{pzt}}s_{\mathrm{p}} + h_{\mathrm{p}}s_{11}^{\mathrm{E}},$$

$$B_{31} = h_{\mathrm{pzt}}^4 s_{\mathrm{p}}^2 + 4s_{11}^{\mathrm{E}} s_{\mathrm{p}} h_{\mathrm{p}} h_{\mathrm{pzt}}^3 + 6s_{11}^{\mathrm{E}} s_{\mathrm{p}} h_{\mathrm{p}}^2 h_{\mathrm{pzt}}^2 + 4s_{11}^{\mathrm{E}} s_{\mathrm{p}} h_{\mathrm{p}}^3 h_{\mathrm{pzt}} + h_{\mathrm{p}}^4 (s_{11}^{\mathrm{E}})^2$$

The term outside the parenthesis of Eq. (26) is actually the capacitance with free boundary condition. Using the dimensions and material properties of the piezoelectric actuator in our design for calculation, it is found that the capacitance with clamped boundary condition is about 30% less than the capacitance with free boundary condition. Although the boundary condition of our case is not exactly the same as that of Kim et al. [16], the results of two cases should be close. For approximation the capacitance with free boundary condition is used here because the resultant estimation of the pump power consumption will be larger, which is safe for our system design. The capacitance with free boundary condition is described as

$$C_0 = \frac{\text{permittivity} \times \text{area}}{\text{distance}} = \frac{\varepsilon_{33}^{\mathrm{T}}\pi b^2}{h_{\mathrm{pzt}}} \quad (27)$$

Suppose the applied voltage is sinusoidal, that is

$$U(t) = U_{\mathrm{m}}\sin(\omega t) \quad (28)$$

The current is then,

$$i(t) = C_0\frac{\mathrm{d}U(t)}{\mathrm{d}t} \quad (29)$$

So, the instantaneous power consumption is given by

$$W_{\mathrm{elec}} = i(t)U(t) = \tfrac{1}{2}\omega C_0 U_{\mathrm{m}}^2 \sin(2\omega t) \quad (30)$$

It should be noted that as a capacitor, the piezoelectric actuator would store a large portion of the input electrical energy; therefore, only part of the input energy can be converted into output mechanical energy for fuel delivery. The stored energy will remain in the driving circuit and will be used in next driving cycle. For the worst case, the maximum value of W_{elec} is chosen to estimate the efficiency of the whole fuel cell system. Combining Eq. (25) and Eq. (30) by eliminating Um, we have

$$\max W_{\mathrm{elec}} = \frac{\pi C_0}{4k_{\mathrm{eff}}^2 f}\left(\frac{\eta^{1/2}+1}{\eta^{1/2}-1}\right)^2 \bar{Q}^2 \quad (31)$$

Here, f is the frequency of the driving voltage.

4. Performance analysis of DMFC

To analyze the performance of DMFC with a micropump fuel delivery system, a model describing the relationship between the flow rate of the liquid fuel and fuel cell *J–V* curve would be more convenient. However, for simplicity, we will use some appropriate experimental data from literature to discuss the performance of fuel cells. Up to now some experimental data have been reported about the performance of DMFC under different operation conditions. For example, Jung et al. [17] evaluated a single cell (7.6 cm^2) performance over the range of 60–120 °C with methanol concentrations of 0.5–4.0 M, flow rates of 9 ml min^{-1}, and an oxygen saturation of 105 sccm. A current density of 230 mA cm^{-2} at 0.55 V was obtained from 2.5 M methanol. Baldauf et al. [18] conducted their experiments under air operation at over low pressure. A current density of 100 mA cm^{-2} and a 0.5 V voltage at 80 °C were observed from 0.5 M methanol. The electrode area of their experimental cells was 3 cm^2. Dohle et al. [19] reported an optimum methanol concentration of 2 M for a 20 cm^2 single cell under 110 °C. The current density and the corresponding cell voltage were in a range similar to that was used by Baldauf et al. [18]. The experiments performed by Amphlett et al. [20] indicated that there is a complex relation between the effect of flow velocity and the influence of the production rate of CO_2.

The latest experimental data on DMFC were presented by Gurau et al. [21]. They measured a series of *J–V* characteristic curves for a single fuel cell assembly (5 cm^2) operating under different operation temperatures (80, 60 and 40 °C), different methanol flow rates (5, 0.5 and 0.15 ml min^{-1}), and different methanol concentrations (2, 1 and 0.5 M). The performance analysis in this paper is mainly based on this group of data. From the data they obtained, it is found that at a low current density (less than 100 mA cm^{-2}), the influence of changing methanol concentration (from 0.5 to 2 M) on the characteristic *J–V* curve of DMFC is not significant. The same phenomenon is also observed from the experimental data obtained by other researchers. Therefore, in our new design, initially a 2 M methanol solution can be added to the cham-

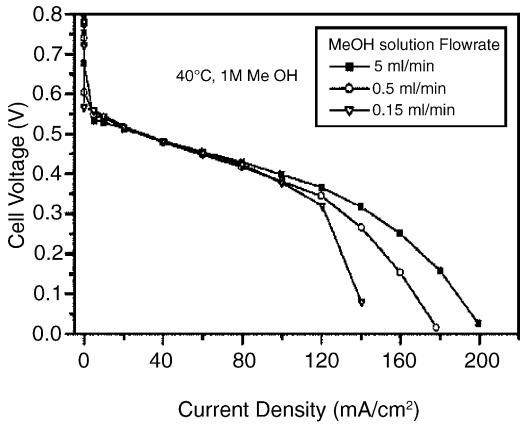

Fig. 4. Selected experimental *J–V* data of a single fuel cell at different fuel flow rate (Gurau et al. [21]).

bers. During operation, the concentration of the methanol solution will decrease due to the fuel consumption. But the performance of the fuel cell will not drop too much if the current density is not very high and the methanol concentration is still larger than 0.5 M. A certain range of methanol concentration can be maintained through continuous fuel flow from the fuel supply manifold.

5. Results and discussions

Fig. 4 shows the experimental data of a single fuel cell running at 40 °C. The concentration of methanol solution is 1 M. The specific data are chosen for calculation because the operation temperature is very close to that of the commercial applications and the concentration is in the middle region. Based on Fig. 4, the power density can be calculated as shown in Fig. 5. The maximum value is reached when the current density is around 120 mA cm^{-2} and the cell voltage is around

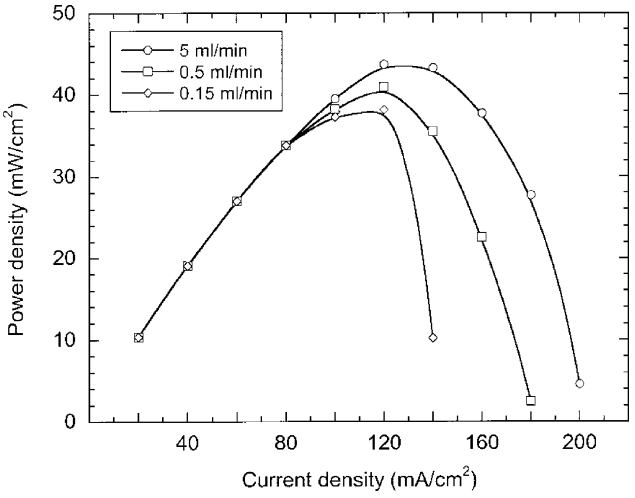

Fig. 5. Calculated power density of a single fuel cell at different fuel flow rate.

0.35 V. If our design is set to be running under this condition, for a 1 W fuel cell assembly, the active area needed is then 25 cm^2 (5 cm × 5 cm) and the total current is about 3 A.

The next thing we need to know is the least fuel flow rate required under this operation condition. As is well known, the electrochemical reactions of a DMFC are:

$$\text{anode reaction:} \quad CH_3OH + H_2O \rightarrow CO_2 + 6H^+ + 6e^- \tag{32}$$

$$\text{cathode reaction:} \quad \tfrac{3}{2}O_2 + 6H^+ + 6e^- \rightarrow 3H_2O \tag{33}$$

$$\text{overall reaction:} \quad CH_3OH + \tfrac{3}{2}O_2 \rightarrow CO_2 + 2H_2O \tag{34}$$

As shown in the above equations, ideally 1 mol methanol will react with 1 mol of water and generate 6 mols of electrons. Therefore, the relation between the total generated current and the flow rate of consumed methanol solution can be described as

$$I = Q \times D_M \times 6 \times F \tag{35}$$

Here, D_M is the mol density of the methanol solution and F is Faraday's constant (96485 C mol^{-1}). Based on Eq. (35), for 1 M methanol, the least fuel flow rate required is approximately 0.31 ml min^{-1}.

The material properties and the dimensions of the micropump actuator are listed in Table 1. As mentioned before, there are two different designs of nozzle/diffuser elements that can be used to direct the flow. Stemme E. and Stemme G. [8] have used one in their valveless micropump, of which the opening angles are small, normally less than 20° and the diffuser direction is the positive flow direction. Gerlach et al. [9] fabricated the other in silicon using anisotropic wet etching. The opening angle of this design is 70.5° and the positive flow direction is in the converging wall direction. In our design, a conical nozzle element with sharp inlet and outlet is chosen due to its easier fabrication process, although the performance is not the best. The opening angle of this nozzle is 70.5°. The minimum diameter is 1 mm and the maximum diameter is 3.15 mm. By following the same analysis method presented by Olsson [7], $\xi_{positive}$ and $\xi_{negative}$ of this nozzle are found to be 1.005 and 1.46, respectively. The ratio of the pressure loss coefficients, η, is then about 1.45.

Since the dimensions and materials of the pump actuator and nozzle/diffuser elements have been determined, the actuation voltage needed to meet the specific flow rate requirement can be calculated by Eq. (25). For example, given the actuation frequency is 100 Hz and the fuel flow rate is 1 ml min^{-1}, U_m is then equal to 71 V. By using Eq. (31), the maximum electrical power consumption is about 70 mW, which is 7% of the total power produced by the fuel cell. Comparing with a similar micropump developed by Bardell et al. [22] that can provide a water flow rate up to 1 ml min^{-1}, while consuming approximately 50 mW power, this estimation is not far away from the real case. Furthermore, some

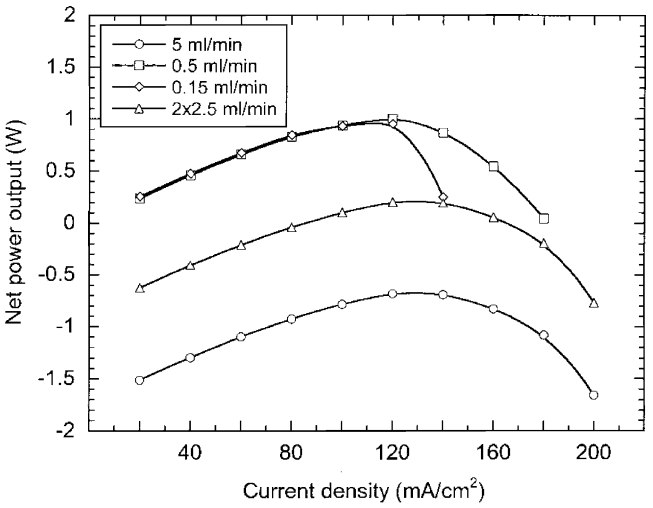

Fig. 6. Net power output under different operation conditions (actuation frequency = 100 Hz).

methods that will be discussed later can be applied to decrease the power consumption of the micropump.

Fig. 6 shows the net output power by subtracting the power consumed by the piezoelectric pump from the total power generated by fuel cell under different operation conditions at a driving frequency of 100 Hz. Data from Fig. 4, which was obtained from the experiments on a 5 cm^2 fuel cell, are used for calculations. So, the results may not be precise but the trend should be similar. The negative output power means that the power generated by fuel cell is not enough to drive the micropump. It is obvious that the fuel flow rate of 0.5 ml min^{-1} is preferred.

From Eq. (31), it can be found that increasing the driving frequency while maintaining the same flow rate can reduce the electrical power consumption of the piezoelectric micropump. Fig. 7 shows the output power curves at a driving frequency of 200 Hz. The fuel cell performance at the

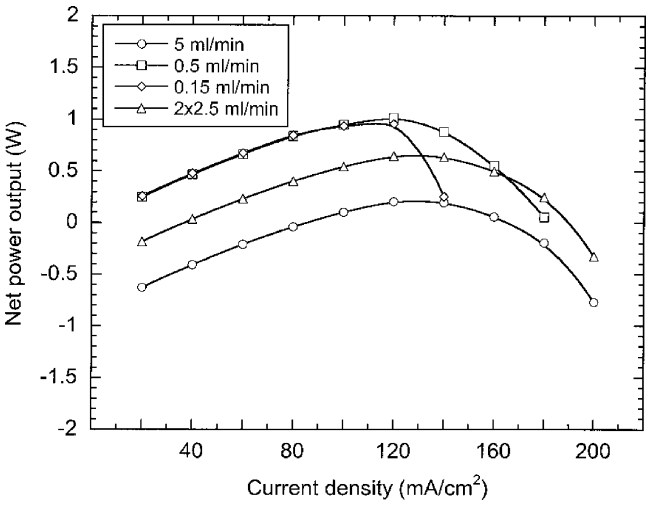

Fig. 7. Net power output under different operation conditions (actuation frequency = 200 Hz).

fuel flow rate of 5 ml min^{-1} is improved but the net power output is still too small. The other way to achieve a high flow rate with a reasonable net power output is by using two micropumps connected in parallel. The performance of two micropumps with a flow rate of 2.5 ml min^{-1} each is also shown in Figs. 6 and 7, which is much better than that of one micropump with a flow rate of 5 ml min^{-1}. However, the trade-off is that the material cost and the system complexity are increased.

When the driving frequency is equal to the resonance frequency, the displacement of the diaphragm will reach the maximum value. After that, to increase the driving frequency further will not improve the pump performance. Also it should be noted that during the high frequency range (close to the resonance frequency), our quasi-static model may not be applicable and a dynamic model need to be established.

Eq. (31) together with Eq. (16) also describes the effects of other factors on the pump power consumption. All these factors are related to the dimensions and material properties of the pump diaphragm structure. It is easily shown that larger R, d_{31} and η values are preferred. Smaller dielectric permittivity ε_{33}^{T} of piezoelectric material corresponds to smaller power consumption. However, the influence of thickness is otherwise quite complicated. Generally speaking, for a specific piezoelectric disk thickness, an optimal diaphragm thickness exists. For some detailed study on the dimensions and material properties of the pump actuator, please refer to Li and Chen [12].

6. Conclusions

In this paper, a viable fuel delivery system using a valveless piezoelectric micropump in a miniaturized direct methanol fuel cell (DMFC) device is presented. A simple analytical pump model combined with some experimental data from the DMFC device is used to evaluate the performance of the fuel cell system. Based on theoretical analysis, the effect of piezoelectric materials properties, driving voltage, driving frequency, nozzle/diffuser dimension and other factors on the performance of the fuel cell system is discussed. It has been demonstrated that with an optimal system design, the piezoelectric micropump only consumes a very small amount of power generated by the fuel cell device. A large driving frequency is suggested to decrease the power consumption of micropump. However, both model improvements and experimental work are needed for further study in the future. It is expected that the design combining DMFC device with piezoelectric micropump for fuel delivery leads to a compact structure of the power generation system for portable electronics.

Acknowledgments

The authors would like to acknowledge the financial support from the Pittsburgh Digital Greenhouse, a State High-

Tech Consortium with research and development focus on System-On-A-Chip technology advancement. This work is also partially supported by University of Pittsburgh Small Grant Funding.

References

[1] C. Hebling, A. Heinzel, U. Groos, Technology and Markets for Portable Fuel Cells, in: Proceedings of the Seventh Grove Fuel Cell Symposium, London, UK, 2001.
[2] M. Waidhas, W. Drenckhahn, W. Preidel, H. Landes, J. Power Sources 61 (1996) 91–97.
[3] K. Scott, W.M. Taama, P. Argyropoulos, J. Power Sources 79 (1999) 43–59.
[4] M.M. Mench, Z.H. Wang, K. Bhatia, C.Y. Yang, Design of a micro direct methanol fuel cell (μDMFC), in: Proceedings of the International Mechanical Engineering Congress and Exposition (IMECE), New York, USA, November 11–16, 2001.
[5] A.K. Shukla, P.A. Christensen, A.J. Dickinson, A. Hamnett, J. Power Sources 76 (1998) 54–59.
[6] K. Scott, P. Argyropoulos, P. Yiannopoulos, W.M. Taama, J. Appl. Electrochem. 31 (2001) 823–832.
[7] A. Olsson, PhD Thesis, Valveless diffuser micropumps, Royal Institute of Technology, Stockholm, Sweden, 1998.
[8] E. Stemme, G. Stemme, Sens. Actuators A 39 (1993) 159–167.
[9] G. Torsten, W. Helmut, Sens. Actuators A 50 (1995) 135–140.
[10] F.K. Forster, R.L. Bardell, M.A. Afromowitz, N.R. Sharma, A. Blanchard, Proceedings of the ASME Fluids Engineering Division, FED, Vol. 234, 1995, pp. 39–44.
[11] A. Ullmann, I. Fono, J. Microelectromech. Sys. 11 (6) (2002) 655–664.
[12] S. Li, S. Chen, Sens. Actuators A 104 (2003) 151–161.
[13] S. Timoshenko, S. Woinowsky-Krieger, Theory of Plates and Shells, second ed., McGraw-Hill, New York, 1959.
[14] A.B. Dobrucki, P. Pruchnicki, Sens. Actuators A 58 (1997) 203–212.
[15] A. Ullmann, Sens. Actuators A 69 (1998) 97–105.
[16] S. Kim, W.W. Clark and Qing-Ming Wang, Proceedings of SPIE, Vol. 5055 (2003) 307–318.
[17] D.H. Jung, C.H. Lee, Chang Soo Kim, D.R Shin, J. Power Sources 71 (1998) 169–173.
[18] M. Baldauf, W. Preidel, J. Power Sources 84 (1999) 161–166.
[19] H. Dohle, J. Divisek, R. Jung, J. Power Sources 86 (2000) 469–477.
[20] J.C. Amphlett, B.A. Peppley, E. Halliop, A. Sadiq, J. Power Sources 96 (2001) 204–213.
[21] B. Gurau, E.S. Smotkin, J. Power Sources 112 (2002) 339–352.
[22] R.L. Bardell, N.R. Sharma, F.K. Forster, M.A. Afromowitz, R.J. Penney, Microelectromechanical Systems (MEMS) ASME, DSC-Vol. 62/HTD-Vol. 354 (1997) 47–53.